Impact of a multi-splitter vane configuration on the losses in a 1.5 turbine stage

T Yasa*, **S Lavagnoli,** and **G Paniagua**
von Karman Institute for Fluid Dynamics, Rhode Saint Genèse, Belgium

The manuscript was received on 12 April 2011 and was accepted after revision for publication on 18 April 2011.

DOI: 10.1177/0957650911409843

Abstract: This study presents the influence of a multi-body architecture on the aerodynamic performance of a low-pressure stator. The novel design has been studied numerically in a one-and-a-half stage turbine by means of a three-dimensional Reynolds-averaged Navier–Stokes simulation. This numerical research compares the behaviour of low-pressure stator composed of two different vanes against a conventional axisymmetric single airfoil row. The computational fluid dynamics predictions were calibrated using experimental aerodynamic measurements. Loss generation mechanisms were evaluated for the conventional and multi-splitter cascades at nominal and off-design conditions. At design conditions, the novel stator and conventional designs show comparable performances. However, the performance is drastically reduced at off-design conditions due to the sensitivity of the structural vanes to flow incidence. This article addresses the performance limitation for the multi-splitter vane configuration and presents a new tool to analyse the non-uniform flow conditions associated with such novel design. This procedure should help researchers in addressing any non-axisymmetric design.

Keywords: turbine flow, performance, aerodynamic, splitter airfoil, numerical research, aerodynamic loss

1 INTRODUCTION

Aero engine designers pursue stringent objectives to increase component efficiency to lower fuel consumption and environmental impacts while reducing engine size, weight, and manufacturing costs. Current design proposals consist of ultra-high bypass ratio concepts [**1**]. An inter-turbine duct with a swan neck or S-shape is used to link the HPT and the LPT (HPT, high-pressure turbine; LPT, low-pressure turbine). In an ulterior attempt to reduce the LPT size, the first stator row is provided inside the duct. In conventional engine designs, the inter-turbine ducts usually host bulky pylons needed to support the engine frame and house service piping [**2**]. These structural components generate high aerodynamic losses.

In this research, a multi-splitter configuration is adopted for the LP stator. The structural pylons, redesigned with an aerodynamic profile, are embedded in a conventional airfoil row. In this study, the performance of such a design is examined and compared with a conventional single-airfoil stator geometry. No public literature exists on multi-splitter configurations applied to aero engine turbine components. Multi-splitter designs have already been applied to radial turbomachinery. In particular, the use of splitter airfoils is common in radial impellers. Miyamoto *et al.* [**3**] performed an experimental characterization of centrifugal impellers with and without splitter blades in which the pressure field and flow angle

**Corresponding author: von Karman Institute for Fluid Dynamics, 72 Chaussee de Waterloo, Rhode Saint Genèse 1640, Belgium.*
email: yasa@vki.ac.be

were presented. Tjokroaminata *et al.* [**4**] performed a design study for a radial turbine with splitter blades. The study shows that the splitter blades give more flexibility for tailoring the loading on the main blades. Asuaje *et al.* [**5**] numerically investigated the effects of splitter blades on the velocity and pressure fields of a centrifugal pump. A 10 per cent increase on the impeller head was documented with the splitter configuration, whereas the pump radial force is amplified by 70 per cent. In axial turbine field, Zhou *et al.* [**6**, **7**] introduced the design concept of the multi-splitter configuration on a steam turbine. Barber and Weingold [**8**] numerically predicted the potential field variation due to the splitter vanes. Kodama and Nagano [**9**] investigated the multi-splitter configuration with variable airfoil pitches. The S-shaped ducts need a novel design, since the flow is likely to separate in such ducts. Miller *et al.* [**10**] carried out an experimental and numerical investigation on the rotor flow migration in an inter-stage diffuser. Axelsson *et al.* [**11**] evaluated the performance of an S-shaped duct downstream of an HPT using flow visualization, directional probes, and pressure taps. Britchford *et al.* [**12**] investigated an outlet guide vane integrated duct at the fan.

In this study, a stator with a splitter vane configuration and without splitter vanes inside a duct is investigated using three-dimensional (3D) Reynolds-averaged Navier–Stokes computation. The simulations were performed at design and off-design conditions. The solver is first calibrated using experimental data. Airfoil loadings and downstream pressure fields are compared for both models. A new methodology is introduced to evaluate the performance of a non-periodic passage flow. The new technique is used to evaluate the pressure loss of both models in terms of global and individual passage performances. The stator geometry with splitter vanes performs similarly to the stator without splitters at design conditions.

2 TURBINE STAGE

The model turbine is a combination of a single-stage HPT and a LP guide vane located in a swan-neck diffuser. The HPT consists of 43 cylindrical stator vanes and 64 3D rotor blades. The innovative LP stator is composed of 16 big aerodynamic cylindrical struts (structural vane) and 48 smaller cylindrical airfoils (aero-vanes), arranged in a multi-splitter configuration. Three small aero-vanes are located in every large structural vane pitch; the resulting four passages are identical in an attempt to maintain the same mass flow distribution as already suggested by Zhou *et al.* [**6**]. The airfoil configuration and the meridional view of the model turbine are depicted in Fig. **1** (left). The big aerodynamic struts and the aero-vanes have the same rear shape to ensure a uniform outlet gas flow. A comparison between the 2D profiles of both the strut and the aero-vane is shown in Fig. 1 (right). The low aspect ratio and the large maximum blade thickness for the strut vanes are imposed by the design objectives. Additional information on the blade row geometry is reported in Table 1 (left). The position of the LP stator with respect to the HPT is reported in Table 2. The geometry of the transition duct has been selected to be a representative of modern engine configurations, and it has a relatively high mean slope of 30° (Table 1, right). This is a good compromise between the geometry for optimal diffusion rate in the duct and the geometry that prevents boundary layer separation, particularly at the tip section.

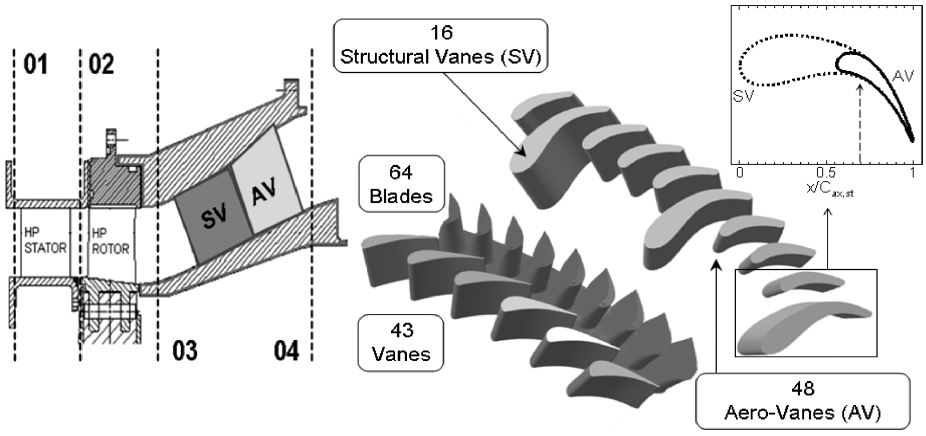

Fig. 1 Meridional view of the test section (left), HPT and LPV 3D view, comparison of strut and aero-vane profiles (right)

Table 1 Summary of the blade row geometries at mid-span (left); inter-turbine diffuser characteristics (right)

	HPT		LPV			
	Stator	Rotor (mid-span)	Strut	Aero-vane	S-shaped duct	
Blades	43	64	16	48	Area ratio (A_{out}/A_{in})	1.3
g/C	0.75	0.75	1.43	0.73	L/H	3
H/C	0.70	1.05	0.52	1.10	Axial length (mm)	172.5
$C_{ax}/C_{ax,r}$	1.03	1.00	2.58	1.14	Mean slope (degrees)	30

LPV, low-pressure vane.

Table 2 Axial spacing between blade rows

Axial gap TE first stator – LE rotor	$0.38 \times C_{s1,ax}$
Axial gap TE rotor – LE strut LPV	$1.15 \times C_{r,ax}$
Axial gap TE rotor – LE aero-vane LPV	$1.56 \times C_{r,ax}$

TE, trailing edge; LE, leading edge.

3 EXPERIMENTAL AND NUMERICAL METHODOLOGY

3.1 Description of the numerical model and test conditions

Experimental investigations were performed at the von Karman Institute compression tube turbine test rig [**13**]. The experimental facility is able to reproduce the actual engine non-dimensional parameters, namely, the Mach number, the Reynolds number, and the blade to gas temperature ratios. A more detailed explanation of the operation of the rig is reported by Dénos and Paniagua [**14**].

The numerical investigation has been performed using the Fine solver [**15**]. Figure **2** displays the two turbine configurations. The first model (Fig. 2, left) is identical to the geometry investigated experimentally. It consists of 36 blocks, covering the nozzle guide vane (NGV) and rotor blade passages plus one strut and three aero-vanes (Fig. 2, left). The struts were replaced with aero-vanes in the second model (Fig. 2, right). Therefore, only 18 blocks (single NGV, rotor blade, and aero-vane) were used to generate the computational domain.

The mesh is generated using around five million and three million grid points for the splitter vane scheme (model 1) and the aero-vane-alone configuration (model 2), respectively. An O-type grid topology was selected around the airfoil, whereas an H-type grid is used in the rest of the domain as shown in Fig. 2 (right).

The steady computation has been performed with a mixing plane approach. The Spalart–Allmaras turbulence model was selected. The calculated value of $y+$ at the airfoil walls is lower than 5. The experimental total pressure and total temperature were imposed as the inlet boundary conditions. The measured static pressure at the hub is used as outlet boundary condition, and radial equilibrium is then applied. A periodic boundary condition is applied at the sides of the domain. Four runs were performed for both models varying the operating pressure ratio of the turbine. The turbine flow conditions of the four operating points are summarized in Table 3. Cases 2 and 4 reproduce two experimental test conditions. The rotational speed of the rotor is the same for the four runs, 6790 r/min.

3.2 Numerical calibration

Pitchwise static pressure distribution is measured at the exit of the rotor and LP stator at 45 per cent $C_{r,ax}$ (plane 3) and 396 per cent $C_{r,ax}$ (plane 4) downstream from the rotor trailing edge, respectively. The measurements are taken for single strut pitches located at two different peripheral locations to monitor the circumferential periodicity. Then, they are duplicated to cover 1.5 pitches. Data are normalized by the inlet total pressure at mid-span to account for test-to-test variations. Pitchwise static pressure distributions measured upstream of the LP stator are presented in Fig. 3. Different symbols are used to distinguish two peripheral locations. The computational fluid dynamics (CFD) predictions for splitter vane model are in good agreement with the experiments both at hub and tip. The strut vane is observed to sensibly alter the aerodynamic potential field close to the rotor outlet. This is due to the large size of the airfoil and its proximity to the rotor blade row. The pitchwise static pressure in plane 3 at the shroud endwall clearly shows a pressure variation (approximately 2 per cent of P_{01}) along a strut vane pitch (Fig. 3). At the hub endwall, the static pressure variation becomes weaker, since the strut leading edge is located further downstream than at the tip.

Figure 4 depicts the static pressure distribution downstream of the LP stator at hub and tip endwalls. The LP stator outlet shows a rather uniform pressure distribution except for case 1 when the second stator outlet is transonic close to the hub region. Numerical predictions indicate that the splitter configuration

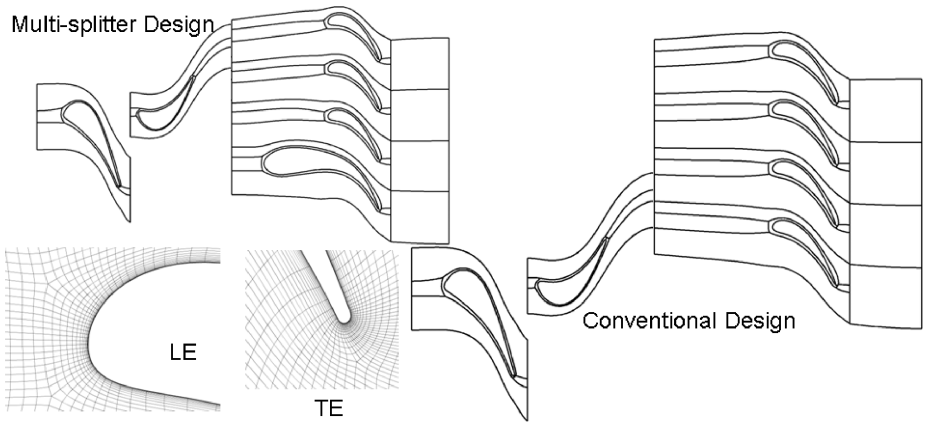

Fig. 2 Numerical domain of multi-splitter design (left), example of grid topology around aero-vane (left-bottom), and numerical domain of conventional design (right)

Table 3 Comparison of some flow quantities at mid-span at different runs

	Multi-splitter design (model 1)						Conventional design (model 2)			
	1	2*	2exp*	3	4	4exp	1	2	3	4
P_4/P_{01}	0.22	0.27	0.27	0.37	0.48	0.48	0.22	0.27	0.37	0.48
P_{03}/P_{01}	0.36	0.38	0.38	0.45	0.55	0.55	0.36	0.38	0.45	0.54
M_{abs3}	0.40	0.37		0.32	0.29		0.40	0.38	0.32	0.30
α_3	−13	−7		12	32		−13	−8	11	30
M_4	0.86	0.71		0.53	0.40		0.86	0.71	0.53	0.41
α_4	64	63		62	59		64	63	63	62

*Design conditions.

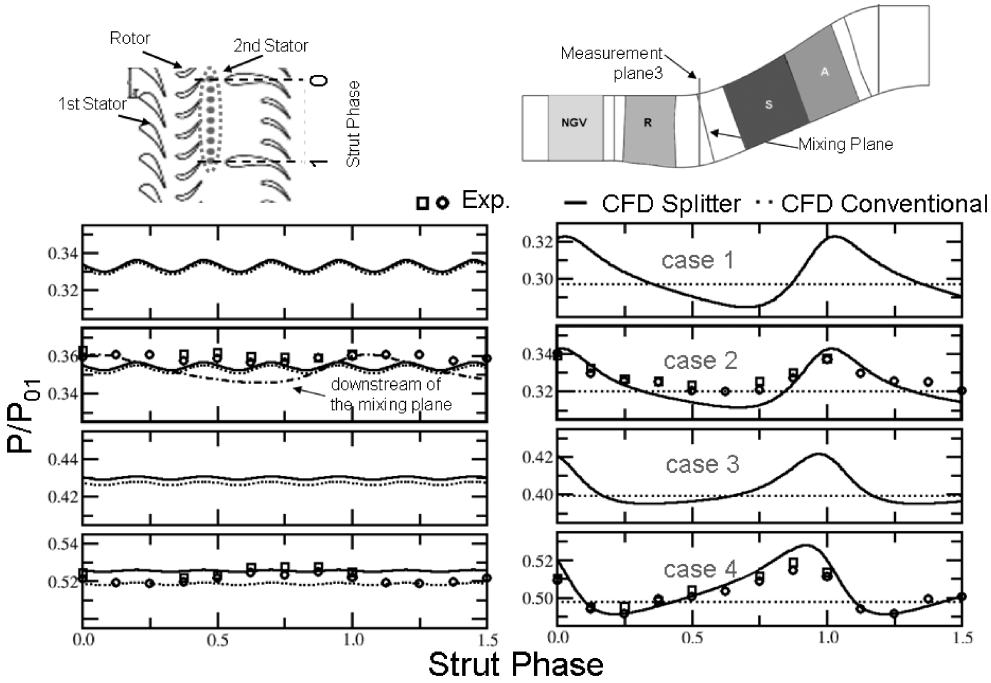

Fig. 3 Pitchwise pressure distribution upstream of the LP stator at hub (left) and at tip (right)

causes a slight variation on the downstream pressure field only at higher outlet Mach number (case 1 – hub). The presence of the strut vane decelerates the outlet speed around the strut phase of 1.

The predicted airfoil static pressure distribution for all cases is plotted in Fig. 5 at mid-span. Good agreement is achieved with the experimental data (cases 2–4). At design conditions (case 2), flow accelerates

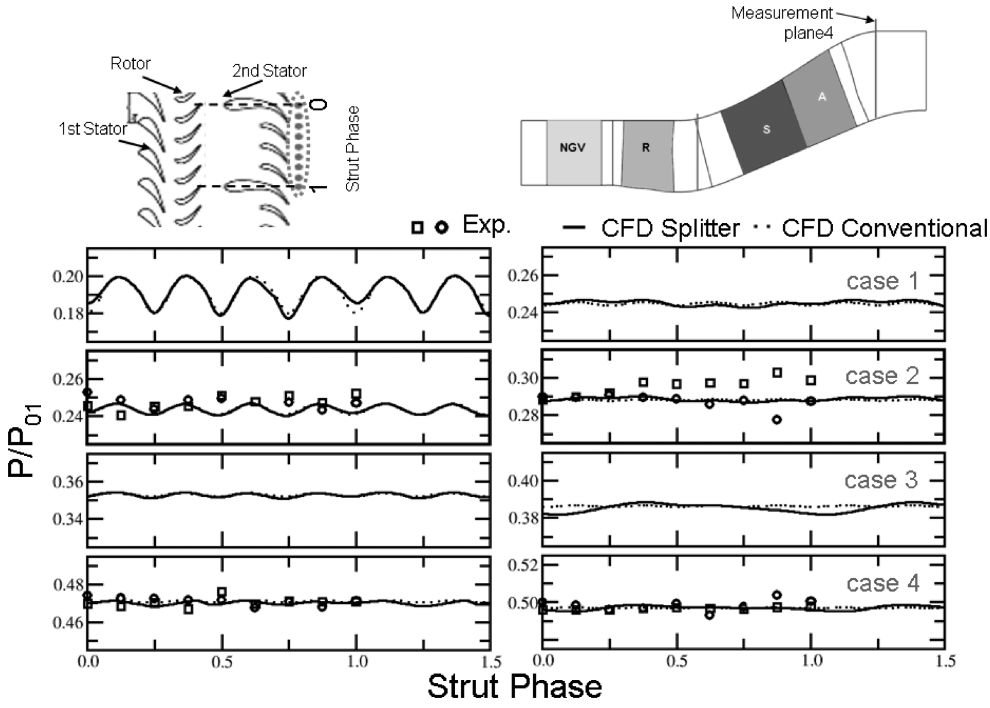

Fig. 4 Pitchwise static pressure distribution downstream of the LP stator at hub (left) and at tip (right)

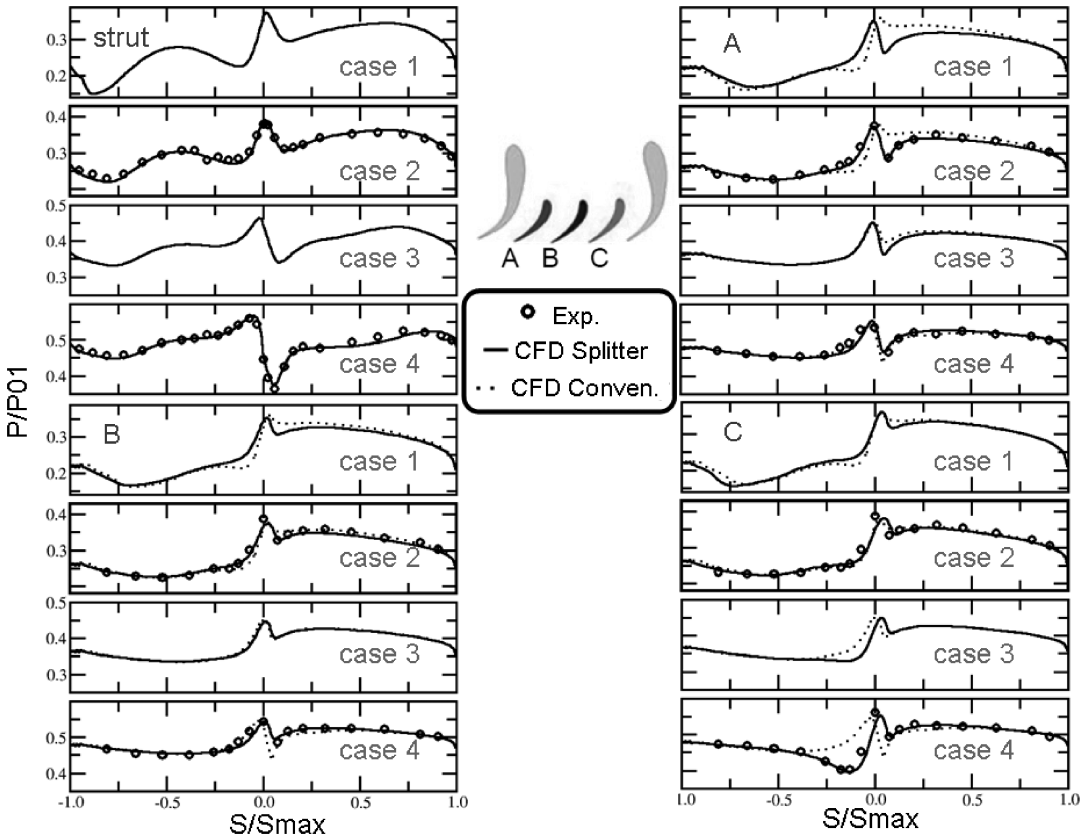

Fig. 5 Static pressure distribution around the three aero-vanes and strut at mid-span

rapidly at the leading edge region because of curvature effect. The flow that enters the strut passage maintains its speed until the aero-vane leading edge. Then, it speeds up into the aero-vane passage smoothly until the trailing edge. Comparison between the multi-splitter and the conventional LPV geometry shows that the strut airfoils primarily affect the flow field in the crown region of the aero-vanes. In fact, the struts modify the incidence angle of the aero-vanes depending on the circumferential position of the aero-vane, since the flow is turned inside the strut passage upstream of the aero-vanes [**13**]. When the stator runs at low-pressure ratio, the incidence angle changes drastically from -7° to 32°, which causes a high diffusion rate close to the shroud due to the existence of the S-shaped duct and leading edge curvature. Therefore, the flow separates on the pressure side of the strut [**13**].

4 INFLUENCE OF THE SPLITTER CONFIGURATION ON THE OUTLET TOTAL PRESSURE FIELD

Figure 6 represents the flow angle difference between the conventional and splitter configuration over a strut pitch. For the conventional model, the flow angle is uniform from the inlet to upstream 10 per cent of the axial chord; from that point onwards, each vane experiences similar distortion. On the contrary, in the splitter model, a variation in the flow angle is caused immediately following the entrance in the strut passage (154 per cent $C_{r,ax}$). However, the outlet flow remains uniform for both configurations, expect for the passage where the separation occurs.

Figures 7 and 8 plot the pressure field 396 per cent $C_{r,ax}$ (plane 4) downstream from the rotor trailing edge. The multi-splitter configuration generates different flow fields at the outlet of each stator passage. The effect of the splitter vane design is easily observed by comparing the total pressure maps of the two flow passages adjacent to the structural vane (S) pressure side (flow passage S-C) and suction side (flow passage S-A). This dissimilarity in the outlet flow field is found to be significant at all the investigated turbine regimes. However, the flow in the passages between the aero-vanes (B-C and A-B) does not suffer any strong change and remains very similar to the aero-vane-alone model. Having positive incidence (case 1) does not have any significant effect on the pressure field. The flow is transonic close to the hub region. The trailing edge shock system causes a low-pressure region. The structural vane shock system has a higher

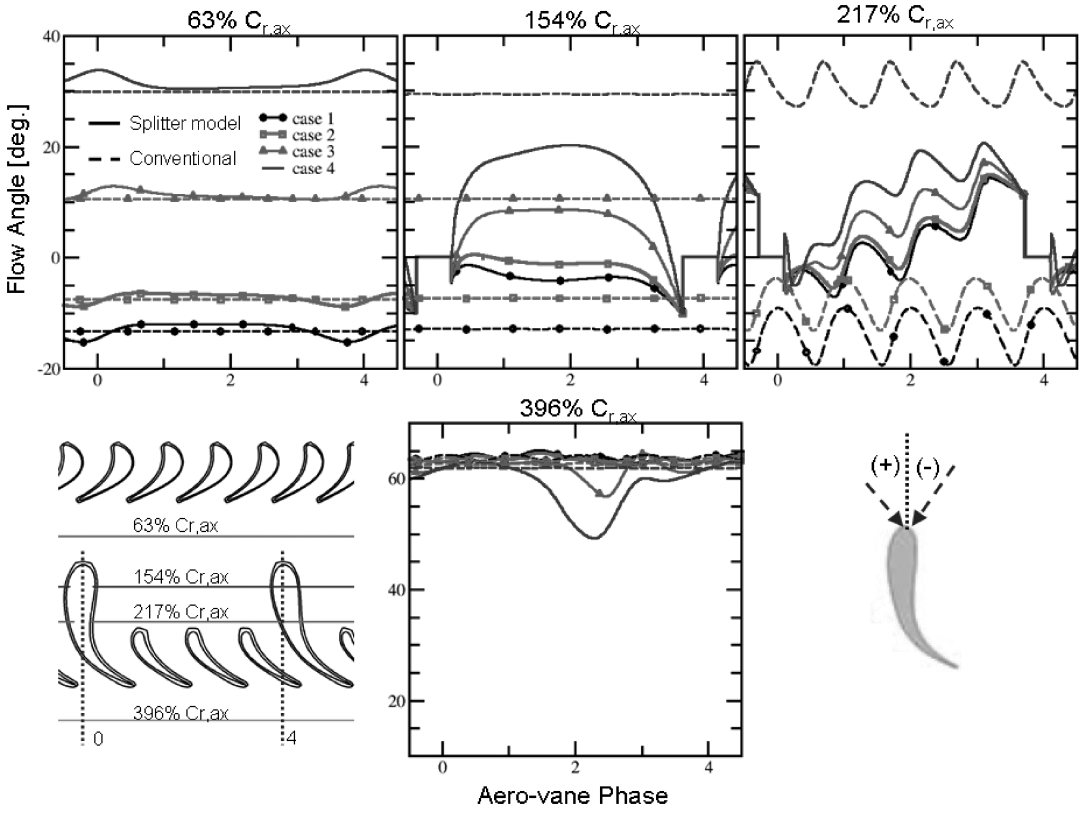

Fig. 6 Pitchwise flow angle distribution for splitter and conventional models

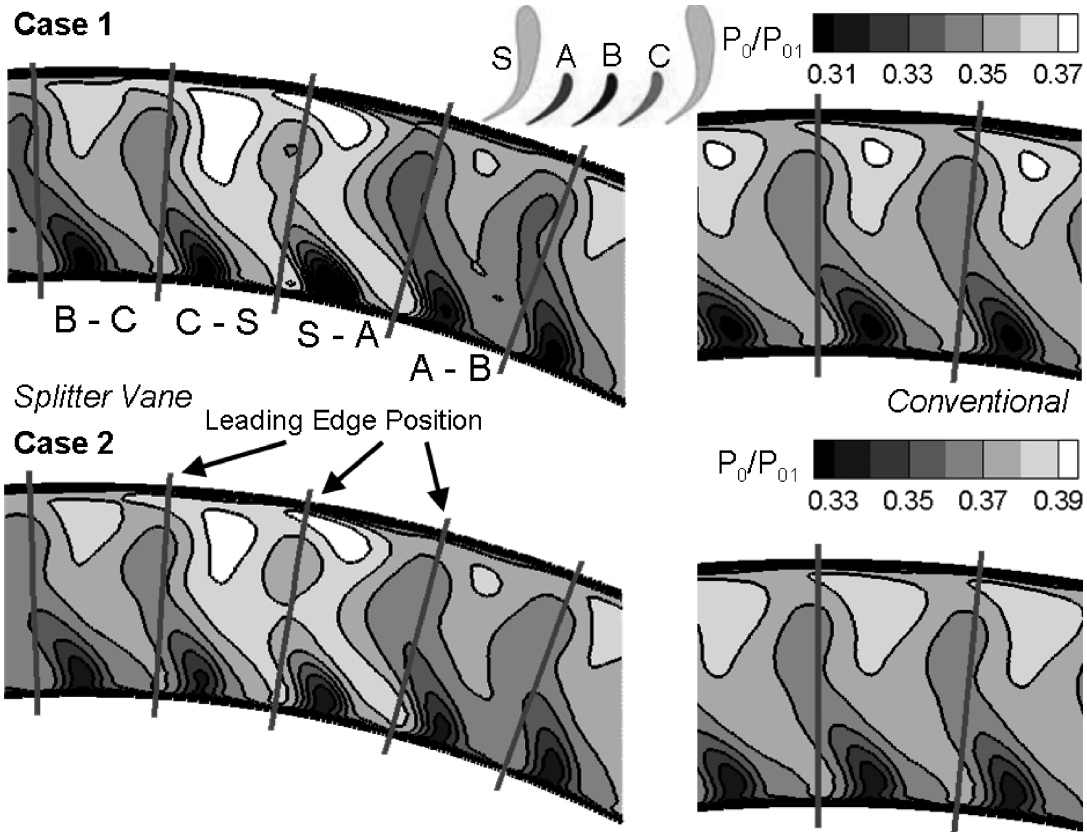

Fig. 7 Non-dimensional pressure field downstream of both numerical models for cases 1 and 2

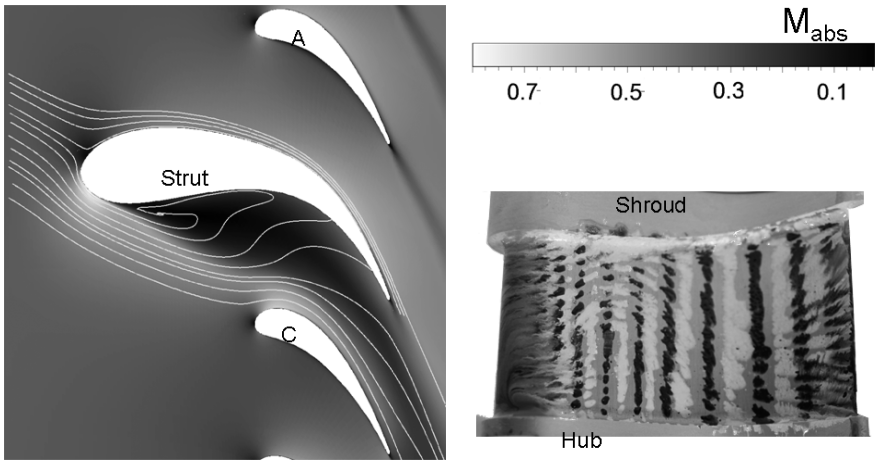

Fig. 8 Mach number distribution and streamlines at 45 per cent of the span for case 4 (left) and flow visualization result of structural vane pressure side (right)

impact to the pressure field when the incidence angle is positive.

The structural vane leading edge region is sensitive in this particular design when it operates with a negative flow incidence (cases 3 and 4). The displacement of the stagnation point towards the suction side, the combination of both the high leading edge curvature of the structural vane and the high diffusion rate at the duct shroud, triggers the flow separation in the passage S-C. Figure 8 (left) shows the Mach number distribution at 45 per cent of the span together with the streamlines. The presence of the recirculation region is also confirmed by experiments, as depicted in Fig. 8 (right).

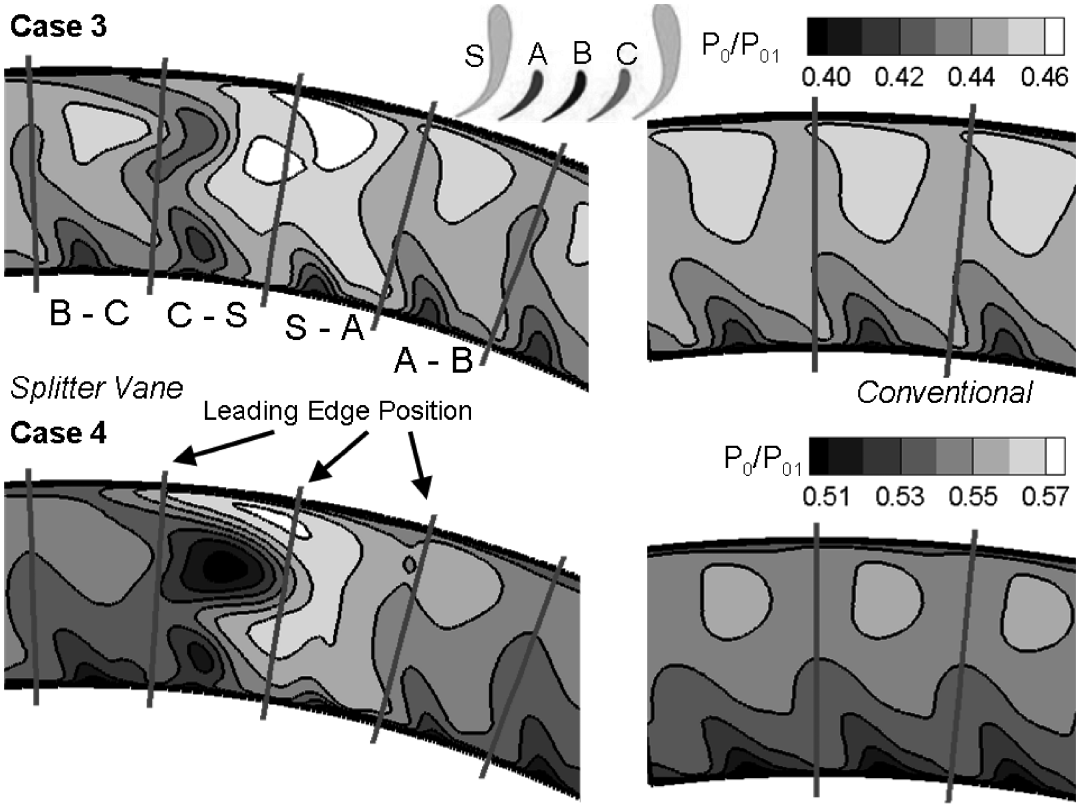

Fig. 9 Non-dimensional pressure field downstream of both numerical models for cases 3 and 4

The separation starts close to shroud region when the flow angle goes from −7° to 12° (case 3), as shown in Fig. 9 (up). This region tends to migrate towards the mid-span when the pressure ratio is lower (case 4). The separation bubble almost blocks the upper half of the channel between the structural vane (S) and vane C. This blockage effect reduces the effective flow area so that the flow accelerates more on the lower half of the passage. On the other hand, the conventional design is free of any separated flow and shows insensitivity to the inlet flow incidence for the investigated off-design conditions.

5 PERFORMANCE EVALUATION AND COMPARISON

5.1 The performance estimation methodology

Traditional performance evaluation methods focus on the flow analysis around an airfoil. However, such approach is not useful for innovative geometries with non-periodic passages. In case of non-periodic flow, a domain comprising of only the ducted passage between the suction side and pressure side of two neighbouring airfoils is considered. The use of this procedure allows the analysis of the streamlines through the passage and the loss associated with them.

The domain limits are defined at the inlet and outlet planes using streamlines on blade-to-blade cuts at 27 different radial locations. Then, at both planes, the rectangular flow channels are generated using the spanwise domain limits of two consecutive blade-to-blade cuts. The radial profiles of the flow properties are obtained by performing pitchwise and mass averaging in each individual rectangular channel. The height of the stream tubes at the inlet and the outlet are adjusted considering a mass flow balance.

5.2 Pressure loss evaluation

The kinetic losses were computed according to Traupel [**16**] shown in equation (1) together with the mass flow distribution along the span for each of the four different vane passages characterizing a full structural vane pitch (splitter vane design). The procedure is then repeated for the conventional design for comparison purposes. Inlet conditions are extracted downstream of the mixing plane. Hence, the inlet plane is slightly shifted downstream of the plane 3, to avoid crossing the interface, where

the mixing plane is located. The outlet conditions are taken at the measuring plane 4 (Figs 3 and 4).

$$\zeta = 1 - \frac{\left(1 - \left(\frac{P_{\text{out}}}{P_{0,\text{out}}}\right)^{\frac{\gamma-1}{\gamma}}\right)}{\left(1 - \left(\frac{P_{\text{out}}}{P_{0,\text{in}}}\right)^{\frac{\gamma-1}{\gamma}}\right)} \tag{1}$$

Figure 10 shows the inlet and outlet mass flow and kinematic loss distributions along the span. The results are depicted for each four individual pitches and for a strut pitch that covers one structural vane and three aero-vane pitches. The performance of each individual passage is compared with the global performance of both the conventional and the new design. The mass flow distributions are normalized by the total mass flow of each passage. The conventional model performs globally better than the new splitter configuration. The performance difference is mainly found above the mid-span. At design conditions (case 2), the aero-vane passages B-C and A-B show similar loss distribution to the 'aero-only' passage. The same consideration holds when comparing the other two passages (A-Strut and C-Strut) up to mid-span. In the upper part of these vane passages, the losses are larger and present the same trend as the 'aero-only' calculation. The loss rise in this region also characterizes the performance of the splitter vane model. When the stagnation point moves towards the pressure side (case 1), the loss profiles do not change significantly. The performance of the passage between strut and aero C is enhanced for the locations above the mid-span. On the other hand, the Strut-A passage shows enhanced loss penalty in the hub region (approximately up to 20 per cent span). This loss rise occurs possibly due to the detrimental effect of transonic flow conditions on the performances associated with this region. The outlet mass flow is equally distributed in the radial direction in both the cases. The structural vane performance is drastically altered when the flow has a negative incidence (cases 3 and 4). A separation region appears at the shroud. The extension of the separation region is proportional to the flow incidence. The recirculation zone obstructs a wide portion of the vane passage adjacent to the strut airfoil pressure side (Strut-C). As a consequence, the radial mass flow distribution is strongly modified not only in the passages next to structural vanes (Strut-A and Strut-C) but also in the passage B-C. Separation causes an increase in the flow speed below the mid-span. Since the inlet mass flowrate is the same as the one at the other passages and the separation region blocks the upper half of the channel, the flow that enters the passage close to the shroud passes between 25 per cent and 60 per cent of the span. Although the performance of the structural

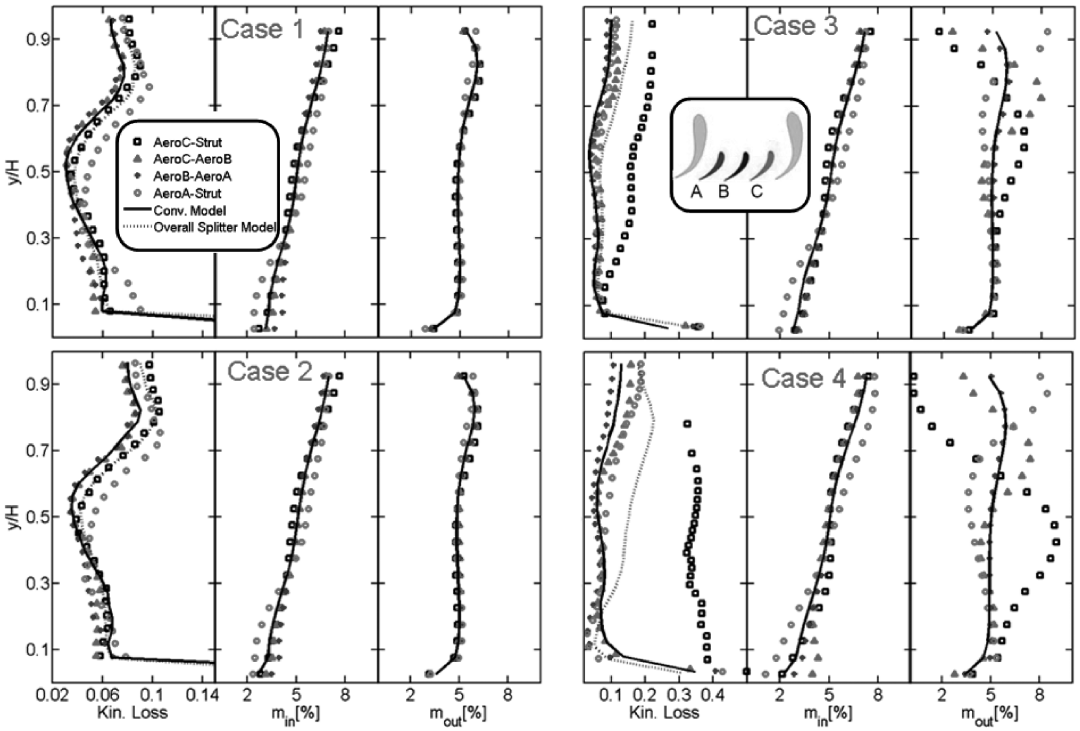

Fig. 10 Kinematic loss and mass flow distribution for all cases

vane is completely penalized by the flow angle change, the maximum variation on the global performance across one structural vane pitch (overall splitter model) is only doubled.

The radial loss distribution is then mass-flow-averaged in order to study the global performance of each passage. Figure 11 displays the global stator kinetic loss as a function of pressure ratio. The results are plotted in two different resolutions (left: high-resolution plot; right: low-resolution plot). The splitter vane configuration shows higher losses for all the operating conditions. However, the performance difference between the two models is less than 1 per cent at design conditions and for positive incidence flow angle. The difference rapidly increases when the flow approaches with a negative incidence. The aerodynamics of the 'aero-vane-only' model is observed to be less affected by large negative flow incidence. The performance of conventional design is unaltered up to an inlet flow angle of 11°. For positive incidence angles, the four aero-vane passages of the multi-splitter configuration generate similar kinetic losses. The performances of the aero-vane passages far from the structural airfoil (C-B and A-B) are improved by the adoption of the splitter vane configuration compared with the conventional model. Since the structural vane passage modifies the inlet flow angle of the aero-vanes, the strong incidence effect is smoothed, and it causes better performance than the 'aero-vane-only' model. The highest increase of the loss is observed for the passage between the structural vane pressure side and the aero-vane suction side (Strut-C). It is about four times higher than the design value at the highest pressure ratio.

6 CONCLUSIONS

An innovative splitter vane configuration is examined using numerical and experimental simulations. A numerical investigation is also carried out using only aerodynamic airfoils in order to identify the flow field differences due to the introduction of a structural vane. The simulations are performed at design and three off-design conditions in which the pressure ratio hence the inlet flow angle is varied. The simulations are validated for two cases using the experimental data.

The flow angle is slightly modified when it enters the structural vane passage. Therefore, the inlet flow angle of each aero-vane along a structural vane pitch is slightly different. It affects the pressure distribution at the front part of the airfoil, whereas the pressure distributions at the rear parts are similar for all the three small aero-vane airfoils. The results for the conventional ('aero-only') model are almost identical to the mid aero-vane (aero-vane B). The structural vane is highly sensitive to the negative incidence. Thus, the splitter vane configuration faces a strong performance penalty due to the generation of separated flow.

The flow passages that are bounded by the aero-vane profiles result in pressure fields similar to the one associated with the 'aero-only' model. The flow separation partially blocks the flow passage on the pressure side of the structural vane at negative-incidence cases. It also modifies the radial mass flow distribution as well as the pressure field in the lower half part of the channel.

The methodology based on flow passages has been introduced in order to estimate the aerodynamic losses. Using this approach, the performances of each passage are evaluated along the span and compared with the global performance of the splitter vane configuration and the 'aero-only' model. A global mass-average loss

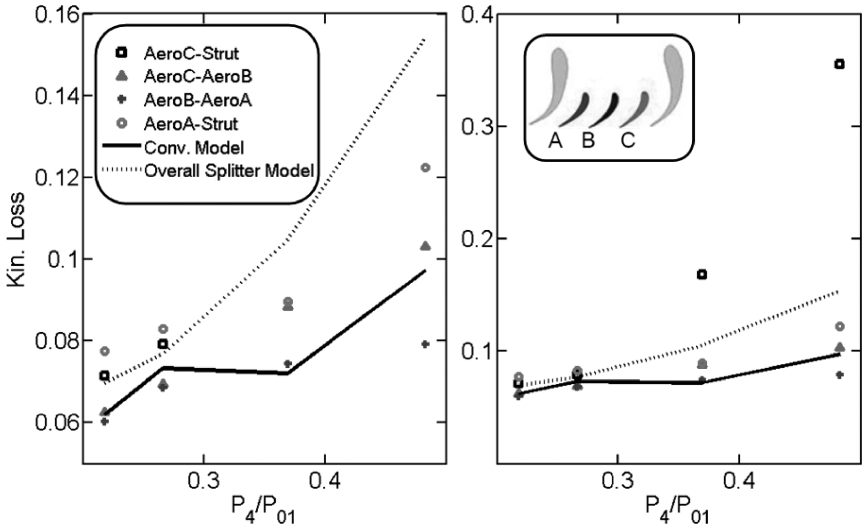

Fig. 11 Variation of the global losses with the operating conditions

is also computed. The two models show similar efficiency levels at design and positive-incidence conditions. When the pressure ratio reduces, the flow becomes locally transonic and penalizes the performance. The splitter vane configuration rapidly loses its performance when the stagnation point moves towards the suction side, whereas the 'aero-only' model can better handle flow angle changes. On the other hand, the structural vane enhances individual aero-vane performance at off-design conditions. This study provides indications to accomplish an efficient design.

ACKNOWLEDGEMENTS

The authors thank Johan Prinsier for his support in numerical investigation.

FUNDING

This research received financial support provided by the European Commission and the industrial manufacturers that participated in the Project TATEF2 (Turbine Aero-Thermal External Flows 2, Grant No. AST3-CT-2004-502924).

REFERENCES

1 **Kurzke, J.** *Aero-engine design: from state of art turbofans towards innovative architectures*, VKI LS 2008-03, 2008 (Sint Genesius Rode, Belgium).
2 **Norris, G., Dominy, R. G.,** and **Smith, A. D.** Strut influences within a diffusing annular s-shaped duct. ASME paper 98-GT-425, 1998.
3 **Miyamoto, H., Nakashima, Y.,** and **Ohba, H.** Effects of splitter blades on the flows and characteristics in centrifugal impellers. *JSME Int. J., Ser. 2*, 1992, **35**(2), 238–246.
4 **Tjokroaminata, W. D., Tan, C. S.,** and **Hawthorne, W. R.** Design study of radial inflow turbines with splitter blades in three-dimensional flow. *ASME J. Turbomach.*, 1996, **118**(2), 353–361.
5 **Asuaje, M., Bakir, F., Kenyery, F., Noguera, R.,** and **Key, R.** 3D quasi-unsteady flow simulation in a centrifugal pump, influence of splitter blades in velocity and pressure fields. In Proceedings of the Sixth European Conference on *Turbomachinery, fluid dynamics and thermodynamics*, Lille, 7–11 March 2005, pp. 562–571.
6 **Zhou, D. M., Zhang, Z. G.,** and **Li, Y. S.** Design and calculation for splintered axial turbine cascade. ASME paper 93-GT-311, 1993.
7 **Zhou, D. M., Zhang, Z. G.,** and **Li, Y. S.** Numerical prediction of profile and endwall losses for multi-splitter turbine cascades. ASME paper 93-GT-255, 1993.
8 **Barber, T. J.** and **Weingold, H. D.** Vibratory forcing functions produced by non uniform cascades. *ASME J. Eng. Power*, 1978, **100**, 82–88.
9 **Kodama, H.** and **Nagano, S.** Potential pressure field by stator/strut interaction. *ASME J. Turbomach.*, 1989, **111**, 197–203.
10 **Miller, R. J., Moss, R. W., Ainsworth, R. W.,** and **Harvey, N. W.** The development of turbine exit flow in a swan-necked inter-stage diffuser. ASME paper GT2003-38174, 2003.
11 **Axelsson, L., Osso, C. A., Cadrecha, D.,** and **Johansson, T. G.** Design, performance evaluation and endwall flow structure investigation of an s-shaped intermediate turbine duct. ASME paper GT2007-27650, 2007.
12 **Britchford, K. M., Carrotte, J. F., Kim, J. H.,** and **Hield, P. M.** The effect of operating conditions on the aerodynamic performance of an integrated OGV and s-shaped duct. ASME paper 2001-GT-0347, 2001.
13 **Lavagnoli, S., Yasa, T., Paniagua, G., Duni, S.,** and **Castillon, L.** Aerodynamic analysis of an innovative low pressure vane placed in a s-shape duct. ASME paper GT2010-22546, 2010.
14 **Dénos, R.** and **Paniagua, G.** *Rotor/stator interaction in transonic HP turbines, VKI lecture series on effects of aerodynamic unsteadiness in axial turbomachines*, VKI LS 2005-03, 2005 (Sint Genesius Rode, Belgium).
15 **Numeca International.** User manual, Fine/Turbo v8.7, 2009 (Brussels, Belgium).
16 **Traupel, W.** *Termische turbomaschinen zweiter band geländerte betriebsbedingungen, regelung, mechanische probleme, temperaturprobleme*, 1977 (Springer-Verlag, Berlin, Heidelberg, New York).

APPENDIX

Notation

A	area (m^2)
C	chord (m)
g	pitch (m)
H	height (m)
L	length (m)
M	Mach number
P	pressure (bar)
S	curvilinear length (m)
α	flow angle (degrees)
γ	heat capacity ratio
ζ	kinetic energy loss

Subscripts

0	stagnation properties
1	turbine inlet conditions
2	high-pressure stator outlet conditions
3	rotor outlet/low-pressure stator inlet conditions
4	low-pressure stator outlet conditions
ax	axial direction
abs	absolute frame of reference
r	rotor blade
st	structural vane